Demeter: Reliable Cross-soil LPWAN with Low-cost Signal Polarization Alignment

Yidong Ren[1], Wei Sun[2], Jialuo Du[3], Huaili Zeng[1], Younsuk Dong[1], Mi Zhang[4]
Shigang Chen[5], Yunhao Liu[3], Tianxing Li[1], Zhichao Cao[1*]
[1]Michigan State University [2]University of California, Los Angeles [3]Tsinghua University
[4]Ohio State University [5]University of Florida

ABSTRACT

Soil monitoring plays an essential role in agricultural systems. Rather than deploying sensors' antennas above the ground, burying them in the soil is an attractive way to retain a non-intrusive aboveground space. Low Power Wide-Area Network (LPWAN) has shown its long-distance and low-power features for aboveground Internet-of-Things (IoT) communication, presenting a potential of extending to underground cross-soil communication over a wide area, which however has not been investigated before. The variation of soil conditions brings significant signal polarization misalignment, degrading communication reliability. In this paper, we propose Demeter, a low-cost low-power programmable antenna design to keep reliable cross-soil communication automatically. First, we propose a hardware architecture to enable polarization adjustment on commercial-off-the-shelf (COTS) single-RF-chain LoRa radio. Moreover, we develop a low-power programmable circuit to obtain polarization adjustment. We further design an energy-efficient heuristic calibration algorithm and an adaptive calibration scheduling method to keep signal polarization alignment automatically. We implement Demeter with a customized PCB circuit and COTS devices. Then, we evaluate its performance in various soil types and environmental conditions. The results show that Demeter can achieve up to 11.6 dB SNR gain indoors and 9.94 dB outdoors, 4× horizontal communication distance, at least 20 cm deeper underground deployment, and up to 82% energy consumption reduction per day compared with the standard LoRa.

*Zhichao Cao is the corresponding author.

ACM MobiCom '24, November 18–22, 2024, Washington D.C., USA

ACM ISBN 979-8-4007-0489-5/24/09…$15.00
https://doi.org/10.1145/3636534.3649358

CCS CONCEPTS

• **Networks** → **Network reliability**; • **Applied computing** → **Agriculture**; • **Hardware** → **Wireless devices**.

KEYWORDS

Agricultural IoT, LPWAN, Cross-soil Communication

ACM Reference Format:
Yidong Ren[1], Wei Sun[2], Jialuo Du[3], Huaili Zeng[1], Younsuk Dong[1], Mi Zhang[4], Shigang Chen[5], Yunhao Liu[3], Tianxing Li[1], Zhichao Cao[1]. 2024. Demeter: Reliable Cross-soil LPWAN with Low-cost Signal Polarization Alignment. In *International Conference On Mobile Computing And Networking (ACM MobiCom '24), September 30–October 4, 2024, Washington D.C., DC, USA.* ACM, New York, NY, USA, 16 pages. https://doi.org/10.1145/3636534.3649358

1 INTRODUCTION

Internet-of-Things (IoT) plays a critical role in precision agriculture [1, 22, 24, 33, 80, 81, 85], in which soil monitoring is an essential part. For example, understanding soil moisture levels in the crop root-zone area can benefit irrigation water efficiency [50]; in-soil nitrate monitoring leads to a deeper understanding of fertilization efficiency [9, 11, 22, 81]. Currently, commercial soil monitoring systems [16, 29, 39] deploy underground soil sensors while leaving communication modules on the ground. However, it is desirable to bury communication modules under the ground as well so that they will not interfere with other agricultural activities (e.g., mowing, harvesting, fertilization, irrigation) [2, 68]. Such *cross-soil communication* has become a key feature of agricultural IoT [45, 70] and has attracted significant interests in recent years [33, 36, 67, 71, 94, 97].

Considering the large-range and long-term deployment in rural farms, rather than ad-hoc wireless sensor networks (WSN) [66–68, 87], Low-power Wide Area Networks (LPWAN) naturally fit to enable agricultural IoT by embracing the wireless technologies featured by low energy consumption and long communication distance [51]. LoRaWAN [3] is a popular LPWAN technology operating on the unlicensed band. It supports long-range data collection from LoRa nodes (typically with sensors) to a gateway. Compared to other cellular LPWAN techniques (e.g., NBIoT [52], LTE-M [37]),

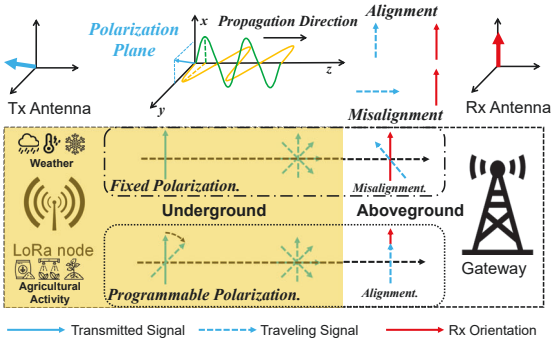

Figure 1: The illustration of polarization misalignment problem (top) and the idea of cross-soil communication and programmable polarization in Demeter (bottom).

LoRaWAN provides a low-cost way to flexibly deploy new infrastructure in rural farm areas where the cellular infrastructure is not available. Some measurement studies [15, 21, 89, 97] have shown the feasibility of adopting LoRaWAN to achieve cross-soil communication. However, achieving a reliable cross-soil LoRaWAN in practice is not trivial. In our in-field measurement (§ 2.1), we observe that the soil condition changes (e.g., moisture, temperature) can lead to a significant signal-to-noise ratio (SNR) variation up to 19.2 dB over a cross-soil LoRa link. Moreover, according to our empirical study of the SNR variation in cross-soil LoRa communication (§ 2.2), compared to the variation of signal attenuation, polarization misalignment between the transmitter and receiver antennas contributes more, leading to 13.2 dB SNR variation. For the available configurations on commercial off-the-shelf (COTS) LoRa nodes [34], such an SNR variation will shorten the communication distance by 4× (§ 5.2) and reduce energy consumption per day by up to 82% (§ 5.3).

The reason for cross-soil polarization misalignment is illustrated in Figure 1. LoRa nodes and gateways adopt low-cost linearly polarized antennas. The polarization (i.e., blue arrows) of an electromagnetic wave emitted from an antenna specifies the geometrical orientation of its oscillations. The received signal power can be maximized if the polarization of the received signal is aligned with the receiver's antenna orientation (i.e., red arrows). However, the soil's microscopic structure and components keep changing over time, subject to different environmental conditions, such as weather and agricultural activity. Consequently, as shown at the bottom of Figure 1, when an electromagnetic wave travels through the soil with complicated scattering, refraction, and reflection [6, 8, 28, 56, 72], its polarization changes over time. Even if the LoRa node's antenna and the gateway's antenna are aligned in advance, the cross-soil transmission can cause polarization misalignment between the received signal and the LoRa gateway's antenna, degrading its power significantly.

Table 1: Qualitative comparison between Demeter and alternative methods regarding COTS compatibility (COTS.), cross-soil reliability, polarization self-alignment capability, and protocol overhead in soil communication. "Pol." and "Dir-Ante." stand for "polarization" and "directional antenna", respectively.

Method \ Challenge	COTS.	Cross-soil Reliablity	Pol. S-alig. Capable	Protocol Overhead
Dual Pol. [38]	*No*	High	Yes	Low
Circularly Pol. [38]	Yes	*Low*	*No*	Low
Dir-Ante. [26, 43]	Yes	*Low*	*No*	Low
Scheduling [35, 91]	Yes	High	*No*	*High*
Demeter (Ours)	**Yes**	**High**	**Yes**	**Low**

There is no prior work on cross-soil LoRa communications for the buried LoRa nodes to send their sensor data to a LoRa gateway over a long distance. We want a solution that is low-cost, interoperable with existing LoRa devices, reliable, and self-adjusting for polarization alignment, with low overhead, such that the LoRa nodes buried underground can operate uninterruptedly for a long time. For low cost and interoperability, we prefer a COTS-compatible solution. Specifically, the LoRa technology is commercialized by Semtech [59] only, with its proprietary radio chips, which all LoRa nodes and gateways in actual deployment use. We say a LoRa node (or gateway) is COTS-compatible if it can be made from the Semtech LoRa radio chips with other (possibly custom-designed) circuitry and computing/storage/signal processing components. A survey of relevant technologies from the literature shows in Table 1 that none of them is satisfactory in meeting all the challenges faced by cross-soil LoRa communications: COTS compatibility, reliability, polarization self-alignment, and low overhead, which we elaborate below.

Challenge 1: COTS Compatibility. There is prior work using a dual-polarized antenna (consisting of two orthogonal polarization antennas) and two RF chains to fully collect the energy of arbitrary polarization signals [38]. Although the work was not directly on LoRa, it is conceivable that its method could in principle be applied on a LoRa gateway to receive polarization-misaligned signals from an underground LoRa node. However, this method is not COTS-compatible because all existing COTS LoRa gateways [61–63] only have one RF chain in their radio chips, not two RF chains required in [38]. Hence, not only does this method carry a higher cost, but it is not applicable to the existing deployments using COTS gateways.

Challenge 2: Cross-soil Reliability. In aboveground and open-space communications, LoRa nodes can utilize circularly polarized antennas, which generate circular polarization signals, to mitigate the polarization misalignment problem [13, 38]. However, the signal reflection, refraction, and scattering of under-ground communications are much more

complex, leading to dramatic axial ratio distortion of circular polarization [42, 75, 82, 83]. This distortion means the wave is no longer circular polarization and can result in a severe signal loss at LoRa gateways, degrading communication reliability [23, 32, 42, 74, 75, 84].

Challenge 3: Polarization Self-alignment Capability. Low-cost electronically switchable directional (ESD) antennas [26, 40, 43, 44], providing antenna gain in a certain direction, can be equipped on LoRa nodes to enhance SNR. However, these directional antennas carry a higher cost in the LoRa band, and they are not capable of mitigating polarization misalignment. Moreover, the antenna gain from low-cost ESD antennas in the low-frequency band is usually too limited to tolerate the observed 13.2 dB SNR variation completely [4, 27, 57, 73, 96].

Challenge 4: Protocol Overhead. LoRa nodes can estimate cross-soil links and schedule transmissions under favorable conditions for good polarization [35, 91]. However, considering the continuously changing soil conditions, maintaining an accurate estimation and scheduling the transmissions may bring considerable computation and energy overhead, particularly for low-cost LoRa nodes.

To address the above challenges, in this paper, we propose Demeter, a low-cost and low-power polarization-programmable antenna system on COTS-compatible LoRa nodes to enable reliable cross-soil LoRa communication. It is inter-operatable with the LoRa gateways in existing deployment. Our key idea is to design a single RF-chain compatible circuit to dynamically adjust the initial polarization of LoRa node transmission. As shown at the bottom of Figure 1, considering the polarization changes during underground signal propagation, the LoRa node adjusts the polarization of its transmitted signal dynamically to ensure the polarization of the received signal is aligned with LoRa gateway's antenna.

The design of Demeter involves three key problems.

First, due to the single RF chain resource on existing LoRa nodes, it is not trivial to design a circuit that enables flexible polarization adjustment. To address this challenge, Demeter uses an RF splitter to split the raw signal from the single RF chain into two signals. In addition, Demeter adopts a dual-polarized antenna, which takes the two signals as the inputs of its two orthogonal polarization dipole antennas to generate a linearly polarized transmission signal. The polarization of the transmission signal can be adjusted by configuring the amplitude ratio of the two signals.

Second, considering the energy constraints on COTS LoRa nodes, energy-exhausting hardware components (e.g., voltage attenuator, amplifier) should not be involved in signal amplitude control. How to control the amplitudes of the two split signals with low-power hardware components is another challenge. To address this challenge, Demeter converts an amplitude ratio to a configurable phase offset between the two signals by utilizing a low-power digital phase shifter and a passive hybrid coupler. The phase shifter adds a preconfigured offset to the phase of one signal. Moreover, Demeter uses the hybrid coupler to mix the two signals to generate two new signals with the corresponding amplitude ratio for the two orthogonal dipole antennas and further customize the hybrid coupler for the LoRa frequency band.

Third, due to the occasional change of the soil condition, the polarization of cross-soil signals is changing over time. To lower link maintenance overhead while keeping agile to the polarization change, when to trigger and how to calibrate the end-to-end polarization alignment between LoRa nodes and gateways are not trivial. To address these challenges, Demeter triggers a calibration process adaptively according to potential soil condition changes in a day. A LoRa gateway initializes a polarization calibration process and asks the targeted LoRa node to transmit multiple beacons with different polarizations. Then we develop a heuristic algorithm to search the best polarization, balancing the searching accuracy and energy overhead on LoRa nodes.

We implement a Demeter prototype with a COTS digital phase shifter [49], a COTS RF splitter [93], a COTS dual-polarized antenna [92], and a customized hybrid coupler on a COTS LoRa node with Semtech SX1276 radio [60]. We have conducted extensive experiments in various soil environments. Our results show that compared with standard LoRa, Demeter can achieve up to 9.94 dB SNR gain outdoors, 4× horizontal communication distance, and at least 20 cm underground buried depth improvement.

In summary, our contributions are summarized as follows:

- To the best of our knowledge, we are the first to develop a reliable cross-soil LPWAN, which is an essential part of agricultural IoT and in-situ soil sensing for realizing precise agriculture in scale.
- We propose a low-cost and low-power polarization-programmable antenna system on COTS single RF chain LoRa nodes. Moreover, we design practical methods to monitor and calibrate polarization alignment over a cross-soil LoRa link with low maintenance costs.
- We implement the prototype of Demeter and evaluate it in real-world deployments. The results show an SNR gain of up to 9.94 dB in real environments, 4× communication distance, and at least 20 cm deeper deployment depth improvement on average. Moreover, Demeter decreases energy consumption per day by up to 82%.

2 PRELIMINARY AND MOTIVATION

LoRa is a wireless communication technology that uses chirp spread spectrum (CSS) modulation to overcome the effects of narrowband interference and multipath fading [58]. This allows LoRa devices to communicate over long distances

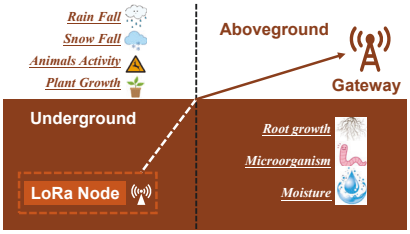

Figure 2: The illustration of cross-soil LoRa communication system.

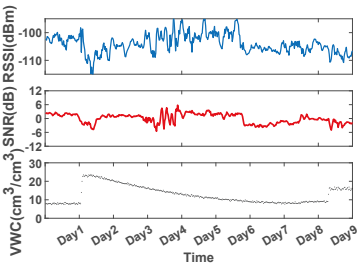

Figure 3: 9-days performance of in-field cross-soil communication.

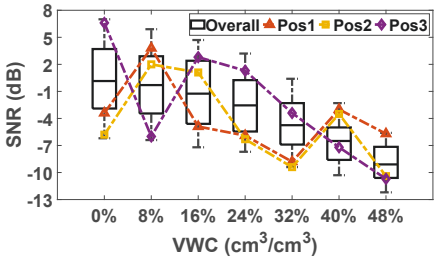

Figure 4: SNR variation analysis across multiple VWC settings.

with low power consumption [51, 76]. Figure 2 illustrates a typical cross-soil LoRa communication system, where LoRa nodes are buried in underground soil and LoRa gateways are deployed in aboveground air. The sensors on the LoRa nodes generate hourly/daily sensory data that is sent to the gateways over a cross-soil link. Many factors (e.g., rainfall, snowfall, temperature, animal activity, plant growth) incur significant soil condition changes over time, leading to unstable cross-soil LoRa links and resulting in packet loss and energy waste.

2.1 In-field Cross-soil Link Measurement

Agriculture soils are categorized into more than ten types, as determined by the ratio of three mineral components (i.e., sand, silt, and clay) according to USDA soil texture document [25, 78]. For example, clay soil consists of more than 50% clay while loam has about 40% sand, 40% silt, and 20% clay. In agriculture, loam soil holds a significant position due to its ideal balance of sand, silt, and clay particles. This balance affords loam soil excellent properties for plant growth, making it highly desirable for farming and gardening.

We conducted a 9-day in-field experiment to explore the quality of cross-soil LoRa communication in a wheat farm. The soil is CvraaB-Conover loam. Its mineral composition is about 40% sand, 40% silt, and 20% clay, respectively [25, 78, 79]. Rainfall comes on Day 2 and Day 9. A moisture sensor [47] connected to a COTS LoRa node is buried at 30cm depth underground, and we deploy a COTS LoRa gateway aboveground. The horizontal distance between the LoRa node and gateway is 10m. The LoRa node sends a soil moisture reading every 30 minutes. The gateway extracts RSSI (Received Signal Strength Indicator), SNR, and VWC (Volumetric Water Content) that measure the ratio of the volume of water to the unit volume of soil from each received packet.

Figure 3 shows the results. From VWC curve, we can observe two rainfalls (i.e., VWC shifting up) on Day 2 and Day 9. Correspondingly, the SNR and RSSI decrease sharply on Day 2 and fluctuate on Day 9. Moreover, we observe another RSSI and SNR drop and fluctuation on Day 6 and Day 4, respectively. Based on the historical weather record, abrupt temperature changes appear these days. Overall, the SNR and RSSI are extremely unstable across 9 days. The RSSI difference reaches to 21.32 dBm. The SNR ranges from 10.4 dB to -8.8 dB. The total 19.2 dB SNR variation verifies that soil condition (e.g., moisture, temperature) changes can degrade communication reliability in real-world deployments.

2.2 Cross-soil Signal Polarization Study

For the cross-soil LoRa link in our in-flied measurement, the observed dramatic SNR variation consists of two parts. One part is from the change of signal attenuation determined by soil's dielectric properties [5, 12, 87] that keep changing along with the changes of soil condition (e.g., moisture, temperature). The other part is from signal polarization misalignment [13]. COTS LoRa nodes and gateways adopt linearly polarized antennas. The polarization of an electromagnetic wave describes the orientation of the oscillating electric field. The electromagnetic wave of LoRa signals is transverse and travels in a specific direction. A magnetic field and an electric field are perpendicular to each other and the direction of propagation. The linear polarization indicates the orientation of the electric field, which oscillates in a fixed plane determined by the magnetic and electric fields and can be purely vertical, horizontal, or any angle in between. When the polarization of the received signals is well aligned with a LoRa gateway's antenna orientation, the energy of the electric fields can be fully captured by the receiving antenna. Consequently, the SNR of the received signals can be maximized. However, in cross-soil communication, signal scattering, reflection, and refraction are inevitable during signal propagation in soils, making the polarization variation at the receiving antenna [7, 30, 46, 64, 72], resulting inevitable polarization misalignment.

We have conducted controlled experiments to investigate the SNR variation incurred by polarization misalignment in cross-soil communication. In an indoor environment, we bury a COTS LoRa node in a plastic container of sandy soil (i.e., > 90% sand) and utilize a COTS LoRa gateway to receive packets. To imitate the soil moisture changes in our in-flied measurement, we change VWC from 0% to 48%. When VWC is 48%, the soil tends to be water-saturated, which only happens when flooding appears in the real world. Thus, we do

not set a higher VWC. To verify the influence of polarization misalignment, for each VWC, we manually vary the polarization of the received signals by uniformly rotating the antenna of the LoRa gateway to 16 different orientations in a plane perpendicular to the direction of electromagnetic wave propagation. For each antenna orientation, the LoRa node will transmit 10 packets. Then, the LoRa gateway collects the packet SNR.

In Figure 4, the five-value boxes show the observed SNR distribution at different VWC configurations. We can see that the SNR variation between the maximum and the minimum SNR under a VWC configuration is 13.2 dB on average. Such a huge SNR variance is purely caused by polarization misalignment. Moreover, for each VWC configuration, the maximum SNR is achieved when the polarization is well aligned. Thus, the changes in the maximum SNR reflect the changes in signal attenuation. We can see the maximum SNR monotonously decreases from 7.0 dB to -5.6 dB, namely the signal attenuation increases 12.6 dB, when VWC increases from 0% to 48%. In our in-flied measurement, the VWC is in the range of [7.8%, 23.1%]. The SNR variation caused by signal attenuation is about 5.8 dB which is 2.3× less than the 13.2 dB SNR variation brought by polarization misalignment. By adding both variations, the total SNR variation is 19.0 dB, which is relatively consistent with the observed 19.2 dB.

Furthermore, we verify that the signal polarization is indeed changed by soil condition change (i.e., VWC increase). The red, yellow, and purple dashed lines represent the SNR of three specific antenna orientations. If the cross-soil signal polarization is constant under different VWC, the trend of the three dashed lines should be similar to the monotonous decrease of the maximum SNR. However, the patterns of the three dashed lines are non-monotonic and totally different. Specifically, the standard deviations of the SNR difference between each dashed line and the maximum SNR are 4.66 dB, 4.2 dB, and 3.78 dB. The dynamic pattern and high deviation verify that the soil condition changes dramatically influence the quality of received signals.

2.3 Motivation

The observed reliability vulnerability motivates us to compensate for the polarization misalignment in cross-soil LoRa communication. On the other hand, a LoRa gateway may cover hundreds or thousands of LoRa nodes. Different LoRa links have diverse polarization misalignments. If we compensate for the polarization misalignment at the gateway side (e.g., rotating the gateway's antenna), the gateway has to assign different LoRa nodes' transmissions at different times. The calibration process, transmission scheduling, and network synchronization will consume considerable energy on LoRa nodes, compromising the energy benefits of the achieved reliable data transmission and incurring new scalability concerns. This motivates us to compensate for polarization misalignment *at the LoRa node side* compatible with the standard LoRaWAN media access control (MAC).

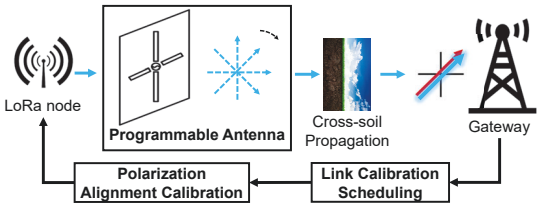

Figure 5: System Overview of Demeter.

3 SYSTEM DESIGN

Figure 5 provides an overview of Demeter. Demeter consists of three parts: 1) the hardware design of a programmable antenna that allows the LoRa node to configure its signal polarization; 2) a polarization alignment calibration algorithm that generates the optimal LoRa node's setting to achieve polarization alignment at the LoRa gateway; and 3) a link calibration scheduling method that optimizes system energy efficiency while keeping communication reliability.

3.1 Hardware Architecture

Figure 6 illustrates Demeter's hardware architecture, which consists of four components as follows:

Passive RF Splitter: To achieve an adjustable polarization degree with only one RF chain and dual-polarized antenna, the first step is to split the single-channel signal into two channels. We use a 3 dB wide-band 2-way passive splitter to divide a signal into two identical signals, each with half the amplitude of the raw signal.

Phase Shifter: An adjustable phase shifter adds a phase offset to the input signal. Demeter adopts a programmable digital phase shifter [49] which can be embedded into COTS LoRa nodes with a 3.3 V voltage supply.

Hybrid bridge Coupler: The hybrid coupler is implemented as a four-ports (i.e., two inputs, two outputs) 3 dB 90° bridge with center frequency at the US915 band for LoRa. A hybrid coupler divides the signal of each input port into two signals with the same amplitude and 90° phase difference, then crossly combines two signals from two different input ports to generate the signals at two output ports.

Dual-polarized Antenna: A dual-polarized antenna consists of two dipole antennas with orthogonal linear polarization orientations and an overlapping geometrical center. The simple structure makes it easy to manufacture and has been widely used in wireless communication.

3.2 Adjustable Polarization Principle

As shown in Figure 6, the raw signal transmitted by a LoRa node is X_0 with amplitude A and phase α, which can be

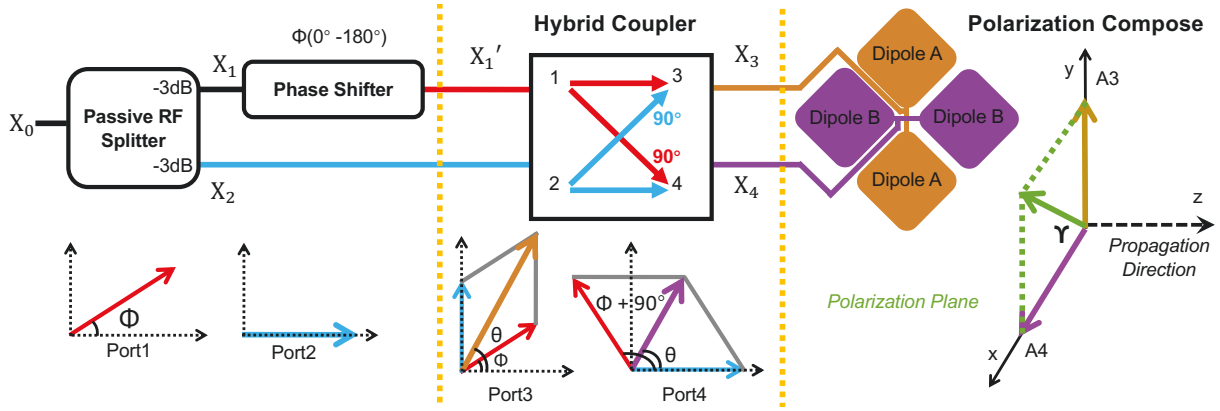

Figure 6: Demeter's hardware architecture and adjustable polarization principle.

expressed as $X = f(A, \alpha, t)$, where t is the time. First, we use the passive RF splitter to divide the raw LoRa signal into two identical signals with half amplitude: $X_1 = f(\frac{A}{2}, \alpha, t)$ and $X_2 = f(\frac{A}{2}, \alpha, t)$. For the first way signal X_1, the digital phase shifter is used to add a phase offset ϕ. We assume the phase shifter is ideal without extra loss, the amplitude of X_1 is still $\frac{A}{2}$. Then we have $X_1' = f(\frac{A}{2}, \alpha + \phi, t)$. We can see that the phase difference between X_1' and X_2 is ϕ, too.

The port1 and port2 of the hybrid coupler take X_1' and X_2 as input, respectively. The output signals at port3 and port4 are X_3 and X_4. To calculate the value of X_3 and X_4, we use X_{ji} to represent the partial output signal at port i from the input signal at port j. As shown in Figure 6, X_3 consists of two parts: X_{32} (i.e., the blue arrow at port3) and X_{31} (i.e., the red arrow at port3). The hybrid coupler adds a 90° phase offset on X_2 to generate X_{32} (i.e., the blue crossing line). Then, X_3 can be calculated as follows:

$$\vec{X_{32}} = f(\frac{A}{2}, \alpha + \frac{\pi}{2}, t) \tag{1}$$

$$\vec{X_{31}} = f(\frac{A}{2}, \alpha + \phi, t) \tag{2}$$

$$\vec{X_3} = \vec{X_{32}} + \vec{X_{31}} = f(\frac{A}{2}, \alpha + \frac{\pi}{2}, t) + f(\frac{A}{2}, \alpha + \phi, t) \tag{3}$$

Port3 vector $\vec{X_3}$ (i.e., the brown arrow in Figure 6) is vectors sum of $\vec{X_{32}}$ and $\vec{X_{31}}$. $\vec{X_{32}}$, $\vec{X_{31}}$ compose a rhombus with same amplitude. Therefore, the phase value of $\vec{X_3}$ should be the mean phase of $\vec{X_{32}}$ and $\vec{X_{31}}$. Let the amplitude of $\vec{X_3}$ be A3. We can simplify $\vec{X_3}$ as:

$$\vec{X_3} = f(A3, \alpha + \frac{\phi}{2} + \frac{\pi}{4}, t) \tag{4}$$

Similarly, X_4 is the combination of X_{42} (i.e., the blue arrow at port 4) and X_{41} (i.e., the red arrow at port 4). Based on X_1', the hybrid coupler adds a 90° phase offset to generate X_{41} (i.e., the red crossing line). We have X_4 as follows:

$$\vec{X_{41}} = f(\frac{A}{2}, \alpha + \phi + \frac{\pi}{2}, t) \tag{5}$$

$$\vec{X_{42}} = f(\frac{A}{2}, \alpha, t) \tag{6}$$

$$\vec{X_4} = X_{41} + X_{42} = f(\frac{A}{2}, \alpha + \phi + \frac{\pi}{2}, t) + f(\frac{A}{2}, \alpha, t) \tag{7}$$

Let us indicate the amplitude of $\vec{X_4}$ as A4,

$$\vec{X_4} = f(A4, \alpha + \frac{\phi}{2} + \frac{\pi}{4}, t) \tag{8}$$

We can see that X_3 and X_4 have the same phase while their amplitudes A3 and A4 are different.

We further feed X_3 and X_4 to the two feeding ports of the two dipole antennas of the dual-polarized antenna. Then the two dipole antennas produce two orthogonal electric fields. Generally, an electromagnetic plane wave that moves in the z-axis direction has two components in x-axis and y-axis [69].

$$E_x = E_{xm} cos(wt - kz + \beta_x) \tag{9}$$

$$E_y = E_{ym} cos(wt - kz + \beta_y) \tag{10}$$

$\vec{E} = \vec{e_x} E_x + \vec{e_y} E_y$ represents for electric field and m means magnitude/amplitude. At the two dipole antennas in the dual-polarized antenna of Demeter, we have two orthogonal electric fields in the x-y plane. Both the wave phases in x and y are equal to $\beta = \alpha + \frac{\phi}{2} + \frac{\pi}{4}$. We set the same z to 0 here.

$$||\vec{E}|| = \sqrt{E_x^2 + E_y^2} = \sqrt{E_{xm}^2 + E_{ym}^2} cos(wt + \beta) \tag{11}$$

$$\gamma = arctan(\frac{E_y}{E_x}) = arctan(\frac{A3}{A4}) \tag{12}$$

According to the principle of vector composition, we can change the amplitude ratio $\frac{A3}{A4}$ between X_3 and X_4 by adjusting the phase offset ϕ to determine the degree of linear polarization γ (i.e., the green arrow at polarization compose). The propagation direction (i.e., black dashed arrow) of electromagnetic waves is the normal of the polarization plane. Finally, we can generate signals with different linear polarization degrees.

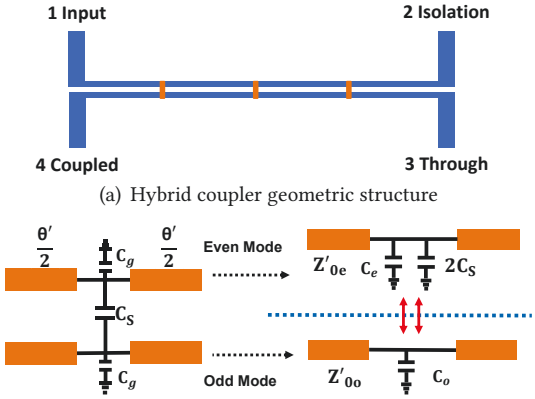

(a) Hybrid coupler geometric structure

(b) Equivalent circuit for each unit cell

Figure 7: The illustration of the hybrid coupler design.

3.3 Coupler Architecture

Some hardware components of our system, such as the phase shifter, the passive RF splitter, and the dual-polarized antenna are COTS devices that can be obtained easily. The hybrid coupler for a LoRa node should be low-cost with a small size without any power supply. However, the sub-1 GHz bridge coupler which meets our demand is limited on the market. Thus, we design the bridge coupler by ourselves.

The purpose of the coupler is to produce 90° phase difference between the signals of two output ports when the input signal is only from one input port and the other one is isolated. Three kinds of RF bridge couplers can achieve the target: codirectional, contradirectional, and transdirectional with different isolated port positions relative to input ports. Compared to the other two solutions, as illustrated in Figure 7(a), a transdirectional coupler can avoid crossover and direct current bias problems because the isolated port and input port are on the same side, making the coupler smaller and scalable for IoT devices [48].

Transdirectional Coupled Line. We adopt an even-odd mode analysis [48] at four ports of the hybrid coupler in Figure 7. Port1 is input and port2 is isolated while port3 is the through and port4 is coupled. V_i (i=1,2,3,4) represents the voltage at port$i$ and V_0 is the generator voltage. Let Z_{in}^e be the input impedance at port1 for the even mode and Z_{in}^o be the input impedance of the odd mode. Z_0 is the load impedance of the transmission line in this coupler.

$$Z_{in}^{(e,o)} = Z_{0(e,o)} \frac{Z_0 + jZ_{0(e,o)} tan\theta}{Z_{0(e,o)} + jZ_0 tan\theta} \tag{13}$$

$$V_1^{(e,o)} = V_0 \frac{Z_{in}^{(e,o)}}{Z_{in}^{(e,o)} + Z_0} \tag{14}$$

According to the symmetrical structure of the transdirectional coupler, the voltage at port4 is

$$V_4 = V_4^e + V_4^o = V_1^e - V_1^o = V_0 [\frac{Z_{in}^e}{Z_{in}^e + Z_0} - \frac{Z_{in}^o}{Z_{in}^o + Z_o}] \tag{15}$$

Based on the definition of Z_{in}

$$Z_{in} = \frac{V_1}{I_1} = \frac{V_1^e + V_1^o}{I_1^e + I_1^o} \tag{16}$$

$$Z_0 = \sqrt{Z_{0e} Z_{0o}} = \sqrt{Z_{in}^e Z_{in}^o} = Z_{in} \tag{17}$$

Combined with Equation 15. N is the coupling coefficient.

$$V_4 = V_0 \frac{j(Z_{0e} - Z_{0o}) tan\theta}{2Z_0 + j(Z_{0e} + Z_{0o}) tan\theta} \tag{18}$$

$$N = \frac{Z_{0e} - Z_{0o}}{Z_{0e} + Z_{0o}} \tag{19}$$

$$V_4 = V_0 \frac{jN}{\sqrt{1 - N^2} cos\theta + jsin\theta} \tag{20}$$

Similarly, we calculate V_3 for port 3 as follows:

$$V_3 = V_3^e + V_3^o = V_0 \frac{\sqrt{1 - N^2}}{\sqrt{1 - N^2} cos\theta + jsin\theta} \tag{21}$$

We can notice that there is always 90° phase difference between V_3 and V_4 due to the same denominator and orthogonal numerator. The scattering parameter S can be computed with voltage ratios ($S_{ij} = \frac{V_j}{V_i}$).

$$S = \begin{bmatrix} 0 & 0 & -\sqrt{1 - N^2} j & N \\ 0 & 0 & N & -\sqrt{1 - N^2} j \\ -\sqrt{1 - N^2} j & N & 0 & 0 \\ N & -\sqrt{1 - N^2} j & 0 & 0 \end{bmatrix} \tag{22}$$

Then, to keep the absolute value of S_{31}, S_{32}, S_{41}, and S_{42} identical for generating the designed X_3 and X_4 signals, we set N as $\frac{\sqrt{2}}{2}$. The S parameter of our coupler becomes:

$$S = \begin{bmatrix} 0 & 0 & -j & 1 \\ 0 & 0 & 1 & -j \\ -j & 1 & 0 & 0 \\ 1 & -j & 0 & 0 \end{bmatrix} \tag{23}$$

Periodically Loaded Design. For a conventional coupled line, we need to satisfy Equation 17 under the necessary constraint of the transdirectional operation:

$$\theta_e - \theta_o = (2n + 1)\pi \tag{24}$$

However, it is challenging to adjust θ_e, θ_o, Z_{0e} and Z_{0o} simultaneously because the spacing between the coupled lines would impact both the impedances and phase velocities. Inspired by transdirectional coupled-line couplers working on 3.6 GHz[65], we adopt periodically loaded coupled lines to overcome this challenge.

We design multiple unit cells with capacitors between coupled lines. The unit cell, consisting of several capacitors and transmission lines, is shown in Figure 7(a). The orange rectangles are patch capacitors. Here N is the number of unit cells. Let θ' be the electrical length of each unit cell and Z_0' the characteristic impedance of the transmission line

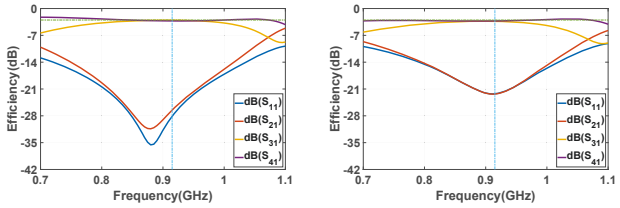

(a) Rogers5880 (b) FR4

Figure 8: Coupler efficiency with different substrates.

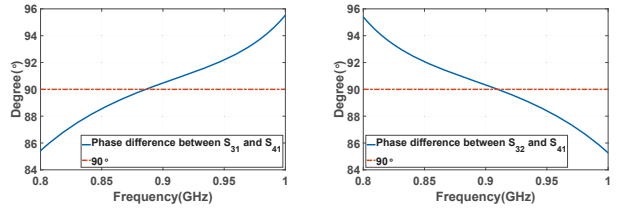

(a) Phase offset for port1 (b) Phase offset for port2

Figure 9: Cross phase shift in Demeter's coupler.

as the equivalent circuit that Figure 7(b) shows. C is the capacitance between the coupler transmission lines. C_g is the capacitance between the coupler and the ground. The shunt susceptances of periodic load on even and odd modes are l_e and l_o. According to the design in [65], we have:

$$cos\frac{\theta}{N} = cos\theta' - \frac{b}{2}sin\theta' \tag{25}$$

$$Z_0 = Z_0'\sqrt{\frac{2sin\theta' + bcos\theta' \pm l}{2sin\theta' + bcos\theta' \mp l}} \tag{26}$$

$$l_{(o,e)} = \Omega C_{o,e} Z'_{0(o,e)} \tag{27}$$

$$C_s = \frac{C_o - C_e}{2} \tag{28}$$

According to Equations 25, 26, 27, and 28, the electrical length for each unit cell can be assigned with a preconfigured value. Then we can calculate the capacitance value of C_s accordingly for the LoRa frequency band.

HFSS Simulation: We use the High-Frequency Structure Simulator (HFSS) to perform electromagnetic simulation on our system. Initially, we use Roger5880 0.5mm thickness substrate with low signal energy loss to ensure high efficiency and verify the system. Figure 8(a) shows the efficiency of the coupler across the four ports in the US915 band. S_{31} and S_{41} can achieve -3.04 dB and -3.24 dB, which are consistent with half amplitude split of X_{31} and X_{41}. And the reflection loss in S_{11} and S_{21} are ultra-low as -28.13 dB and -26.52 dB, achieving high energy efficiency. However, Rogers5880 is expensive hindering us from deploying Demeter on a large scale. In addition, Rogers5880 is too soft to be distorted easily, causing unexpected circuit changes and high loss.

To benefit IoT deployment, we redesign our coupler with substrate FR4 at 1.6mm thickness, which is one of the cheap, hard, and easily processed substrate materials. In HFSS, by

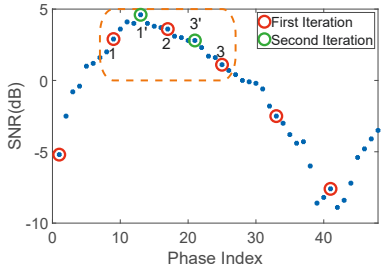

Figure 10: The illustration of peak search algorithm of Demeter for polarization alignment calibration.

adjusting the geometrical shape and parameters like electrical length, bridge width, and capacitors, we successfully achieve a 90° phase offset with low loss as shown in Figure 9. The phase difference between S_{32} and S_{42} range from to 89.85° to 90.22° in the US915 band and S_{32} and S_{42} range from to 90.6° to 90.92°. Figure 8(b) shows that S_{31} and S_{41} are -3.35 dB and -3.24 dB. And the reflection loss in S_{11} and S_{21} are -22.23 dB and -22.29 dB, still very low levels. The performance is comparable with Roger5880.

3.4 Polarization Alignment Calibration

The calibration problem is to find the optimal phase offset configuration of the phase shifter that makes the signal polarization aligned between a Demeter node and a LoRa gateway, namely the observed SNR is the highest at the LoRa gateway. Instead of traversing all possible phase offset configurations, we design a heuristic SNR peak searching algorithm to minimize the control overhead.

SNR Peak Searching Problem: The digital phase shifter can provide n different discrete phase offsets, which generate different polarization degrees of the output signal. We use the term "phase index" (i.e., from 1 to n) to represent these phase offsets in ascending order. We aim to find out the phase index that enables polarization alignment, namely obtaining the highest SNR at the gateway side. Intuitively, a LoRa node can send n probing beacons that cover all available phase indexes to a LoRa gateway. Then, the gateway feedbacks the one with the highest SNR to the node. For example, in Demeter prototype, we have 45 phase indexes. Figure 10 shows the SNR changes (e.g., blue dots) for a cross-soil link deployed in the real world. We can see phase index 13 with the highest SNR 4.6 dB should be selected.

Heuristic Calibration Algorithm: Demeter transmits beacons with varied polarizations in a short duration. The cross-soil communication links are quite stable during a short period [55, 88]. Therefore, in Figure 10, the SNR changes comply with a sine wave approximately, where only one valley and one peak exist. By noticing this property, we can reduce the transmission number of probing beacons of current SF in a heuristic way. The algorithm contains two parts. First, we use six uniformly distributed phase indexes to determine the

(a) Implementation. (b) Coupler (c) Experiments deployment on a wheat farm

Figure 11: The implementation of Demeter prototype and experiment environments. The box containing a battery, a LoRa node, and our prototype of Demeter RF components is buried in loam soil at the top right corner of subfigure (c). Moisture experiments with additional moisture sensor are shown in the bottom right corner of (c).

optimal phase index's range. Then, we use binary search to find the optimal phase index in this range iteratively. For example, Figure 10 shows that the LoRa node first transmits six probing beacons using the phase indexes marked by the red circles. The gateway feedbacks that the optimal phase index is in the range of either [1,2] or [2,3]. Then, the node sends another two probing beacons with phase indexes 1' (i.e., the middle of [1,2]) and 3' (i.e., the middle of [2,3]). The gateway feedbacks that the new search ranges [1',2] and [2, 3']. The node and gateway repeat this process to find the optimal phase index. In practice, we control the number of iterations to balance the polarization accuracy and the energy cost at the node side.

3.5 Link Calibration Scheduling

In our empirical study in Section 2.1, we observe that the SNR of a cross-soil LoRa link is influenced by the changes in soil conditions (e.g., moisture, temperature) significantly. When soil conditions change, the SNR is also degrading or fluctuating. With this observation, we need to trigger link calibration more frequently if soil conditions change fast. In Demeter, LoRa nodes and gateways periodically trigger the polarization alignment calibration Θ times in a day. If the soil condition (e.g., rainfall, snowfall, fertilization, irrigation) changes frequently, we set a large Θ. Otherwise, we keep Θ small to reduce the energy costs. Therefore, based on the weather report, agriculture activity plan, and soil sensory data, we empirically configure Θ every day.

4 IMPLEMENTATION

We implement a prototype of Demeter[1] with three COTS hardware modules and a customized hybrid coupler operating on the US915 band. The COTS hardware modules include a 3 dB XRDS-RF 698-2700MHz passive RF splitter [93], an ANT627-NF-PANEL-MIMO-OD [92] dual-polarized antenna, and a digital phase shifter PE44820 [49] with 45 available phase offset indexes. Considering the loss of the phase shifter, we apply another identical one with no phase offset to the other signal, balancing the strength of the two split signals.

We implement the hybrid coupler on two kinds of substrate: FR4 with 1.6 mm thickness and Rogers5880 with 0.5 mm thickness. The 0402 patch capacitors with values of 4.3pF and 3.3pF are used in Demeter on the Rogers5880 and FR4 coupler, respectively. As shown in Figure 11(b), the length and width are 63 mm and 25 mm, which is a relatively compact size for the IoT device working in sub-1G frequency. We use a vector network analyzer to measure the S parameters of our hybrid couplers. The phase difference between S_{31} and S_{41} is 89.6° and the phase difference between S_{32} and S_{42} is 90.7°. The signal loss of Demeter is 1.5 dB. The extra transmission power consumption of Demeter is 600 μW, which is neglectable compared with COTS LoRa nodes' tens of mW transmission power. Moreover, since we use a wide-band dual-polarized antenna and phase shifter, the total cost of the Demeter prototype is 150 US dollars. We can lower the cost to about 20 US dollars by integrating all these modules into a unified circuit with a US915 band RF-front. The cost can be further lowered with volume production.

As Figure 11(a) shown, we implement a Demeter node by connecting Demeter to a COTS LoRa node with Semtech SX1276 radio chip [60]. For LoRa gateways, we use UHD and GNUradio to control a USRP N210 [54] with an SBX 400-4400 RF daughterboard [53]. We also use a COTS LoRa gateway with Semtech SX1302 radio chip [61] and SoilWatch 10 moisture sensor [47]. We implement the polarization alignment calibration algorithm using the standard LoRaWAN Class A MAC, which is the default and most energy-efficient one. We run a heuristic algorithm script at the gateway to evaluate the SNR from the LoRa node in soils. We set RECEIVE_DELAY as 10 s to give enough response time for the gateway to generate feedback. We adopt 2 iterations and send 7 probing beacons in total in each calibration process. At the receiving window, the LoRa node turns off the phase shift function but keeps receiving signals through the phase shifter, which does not influence the signal reception.

[1]The source design are available at *https://github.com/YDRen001/Demeter*.

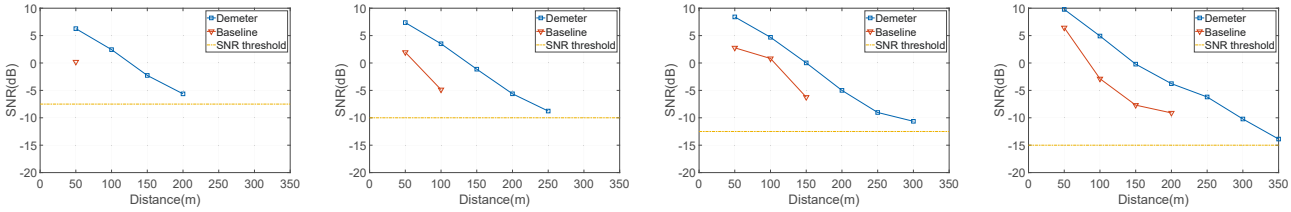

(a) SF=7 (b) SF=8 (c) SF=9 (d) SF=10

Figure 12: Impact of horizontal distance to Demeter.

5 EVALUATION

We evaluate the communication reliability of Demeter in both indoor and in-field environments. In addition, we demonstrate the energy efficiency of Demeter regarding different calibration trigger frequencies.

Performance Metrics: We use two metrics to evaluate the performance of Demeter. The first is **SNR** of the received packets, which is a widely used metric in wireless communication to indicate communication reliability. The higher the observed SNR is, the more reliable the communication is [19]. All the SNR gain values are net gain. The second is **Energy Consumption per Day**. We use Joule per day (J/Day) to present energy consumption under various settings.

Baseline Method: We compare Demeter with the default linear polarized antenna without polarization alignment. In our implementation, we only use one dipole antenna of the dual-polarized antenna to generate the baseline signal with the same power as Demeter.

5.1 Indoor Experiment

Experiment Settings: We conduct indoor experiments to verify the SNR gain of Demeter in polarization alignment for cross-soil communication. We bury a Demeter node in a plastic container of sandy soil and utilize the COTS LoRa gateway to receive packets as Figure 11(a) shown. The distance between the antenna and the gateway is 20 m and the in-soil distance between the antenna and the edge of the container is 0.6 m. Then we gradually add water and stir the soil evenly to change VWC from 0% to 48%. For Demeter, we calibrate the polarization, and the antenna orientation is randomly placed, then we calculate the average SNR of 10 packets. For the baseline method, we collect and estimate the SNR of 10 packets from the LoRa node for each of the 16 different orientations of the manually rotated antenna of the LoRa gateway. For each VWC level, we keep the same wireless link between the two methods by switching the transmitter connected to the antenna ports without changing soil conditions. The spreading factor (SF) of LoRa transmission is 10.

Results: Table 2 shows the maximum (i.e., Max SNR) and minimum (i.e., Min SNR) SNR values of the baseline method at different antenna orientations and the average SNR value of Demeter at different VWC levels. We can see that the Demeter's SNR is 0.21 dB higher than Max SNR on average.

Table 2: Comparison between COTS LoRa devices and Demeter performance in sandy soil with different moisture levels. The metric is SNR with unit dB

VWC (cm^3/cm^3)	0%	8%	16%	24%	32%	40%	48%
Max SNR	5.9	5.2	5.7	3.2	0.2	-2.6	-6.1
Min SNR	-5.9	-6.5	-7.2	-7.7	-9.6	-10.6	-12.7
Demeter SNR	6.1	5.1	6.0	3.3	0.5	-2.1	-5.9

Moreover, Demeter SNR can achieve 11.6 dB SNR improvement compared to Min SNR. The results indicate that Demeter can achieve good polarization alignment to maintain high communication quality compared to manual polarization alignment adjustment.

5.2 In-field Experiment

We evaluate the performance of Demeter under five different configurations in terms of environment and deployment outdoors. We conduct experiments on a wheat farm as shown in Figure 11(c). In the experiments, we dig a hole and bury a battery, a LoRa node, and our prototype of Demeter RF components (as mentioned in Section 3) in a plastic box to protect devices. Considering the potential ultra-low SNR outdoors, we utilize the USRP as the gateway to collect raw signals and compute average SNR among multiple symbols. After the polarization alignment calibration, we collect 12 packets to measure the average SNR value for Demeter. For the baseline, we also collect 12 packets to measure the average SNR. We set a 45° inclined antenna (Figure 14) of the gateway towards to underground node in baseline and Demeter. The default moisture is 11%, and the default soil type is loam soil.

1) Horizontal Distance Experiment Settings: As shown in Figure 11(c), we conduct experiments in multiple horizontal distances from 50 m to 350 m. Orange triangles represent the locations of the gateway at various distances. The blue star is the location of the buried node. The buried depth is 35 cm. We set different SFs from 7 to 10 in the experiments.

Results: As Figure 12(b) and Figure 12(a) shown, compared to the baseline, the SNR gain of Demeter is at least 8.87 dB and 9.94 dB with SF-8 at 150 m and SF-7 at 100 m respectively. The average SNR gain of SF9 and SF10 are 6.16dB and 6.55dB, respectively. The average SNR gain of Demeter achieves 6.86 dB across different configurations. We can observe that the SNR difference between Demeter and the baseline varies because the polarization of the baseline is

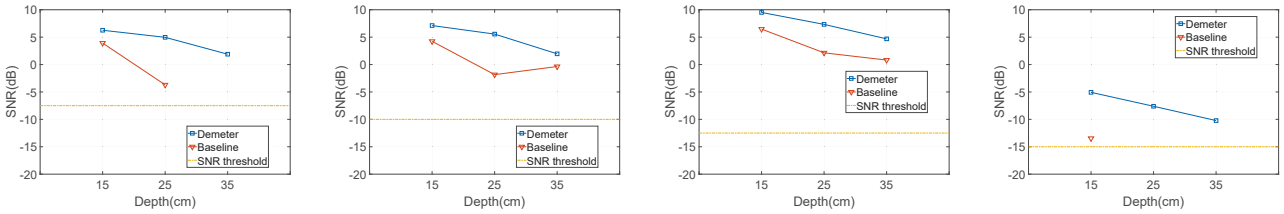

(a) SF=7, Distance=100m (b) SF=8, Distance=100m (c) SF=9, Distance=100m (d) SF=10, Distance=300m

Figure 13: Impact of depth to Demeter.

Figure 14: The three different antenna orientations.

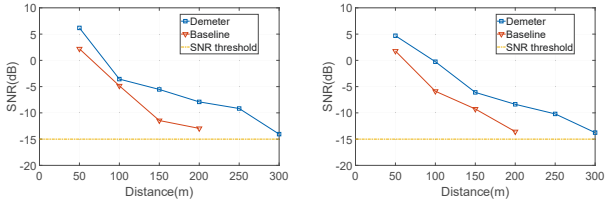

(a) vertical (b) horizontal

Figure 15: Impact of antenna orientations to Demeter.

random when Demeter achieves polarization alignment. Due to terrible polarization, the baseline signals may drop lower than the required SNR for successful decoding. Standard LoRa may increase SF to adapt. Instead, Demeter can recover wireless communication without varying SF. In Figure 12, if the distance is beyond 250 m, the baseline suffers from misalignment polarization, and Demeter trigger polarization alignment calibration to improve the signal SNR from under threshold to above threshold. Every time SF is added by one, the distance of Demeter can be enlarged by 50 m. For SF7, SF8 and SF9, distance promotion is 4×, 2.5×, 2× and 1.75× respectively in the Figure 12(a), Figure 12(b) , Figure 12(c) and Figure 12(d). Based on the results, Demeter can achieve 2.5× communication range on average compared with COTS LoRa. It is equivalent to a 6.56× coverage area gain.

2) Depth Experiment Settings: To verify the performance of Demeter in different underground depths, we placed the Demeter node into three depth levels underground, 15 cm, 25 cm, and 35 cm, as SF is set from 7 to 10. We evaluate Demeter under the horizontal distance as 100 m and 300 m.

Results: Figure 13(a), Figure 13(b), and Figure 13(c) show the results. In all settings, we can see the SNR gain of Demeter compared to the baseline. Under 300 m horizontal distance and SF-10, the baseline signal can be detected only when the depth is 15 cm. Demeter make the LoRa signal appear again when depth is 25 cm or 35 cm as shown in Figure 13(d). The depth of Demeter can be extended to 2.33× compared with the baseline. In Figure 13(b), the SNR gain is only 2.2 dB at 25 cm depth while the SNR gain is 8.67 dB with 35 cm depth. This indicates the wireless link is unstable when depth changes. The average SNR gain of Demeter achieves 5.30 dB across different configurations. Besides horizontal distance, Demeter can also improve maximal soil depth by polarization alignment calibration for cross-soil wireless communication.

3) Antenna Orientations Experiment Settings: The different antenna orientations of the gateway can influence the polarization alignment directly. In this experiment, the gateway antennas with vertical and horizontal orientations are selected to explore the impact of antenna orientation for Demeter. SF is set as 10, and the depth is 35 cm. Figure 14 shows the three kinds of antenna orientation.

Results: The measurement results are illustrated in Figure 15. We can observe that compared to the baseline, the average SNR gain of Demeter in the vertical antenna (Figure 15(a)) is 6.41 dB, which is close to the 6.34 dB SNR gain of the horizontal antenna (Figure 15(b)), and 6.55 dB of 45° inclined antenna in Figure 12(d). This verifies that even if the gateway antenna is put in different orientations suffering from beam mismatching and polarization plane changes, Demeter can work perfectly to provide reliable communication.

4) Moisture Experiment Settings: We explore the impact of different moisture levels (11%, 16%, 25%, 36%, 47%). We use a moisture sensor to measure the VWC before we bury Demeter node underground. The measurement depth of VWC sensor and Demeter node is 35 cm. SF is set as 10.

Results: As illustrated in Figure 16, the average SNR gains with 16% VWC and 25% VWC are 6.41 dB and 6.24 dB respectively compared to the baseline. Both values are close to 6.55 dB gain in Figure 12(d) with VWC 11%. The SNR gains decrease slightly due to VWC growing up as the attenuation also increases. The SNR gains in Figure 16(b) range from 3.54 dB to 8.64 dB while SNR gains range from 4.25 dB to 8.49 dB in Figure 16(a). With higher moisture levels in Figure 16(c) and Figure 16(d), the overall SNR decreases because of the moisture-caused attenuation. But Demeter can still compensate 5.29 dB SNR on average when VWC=36% and enlarge 4× horizontal distance in flooding status with VWC=47%. This indicates Demeter can accommodate different soil environments with various moisture conditions to achieve polarization alignment.

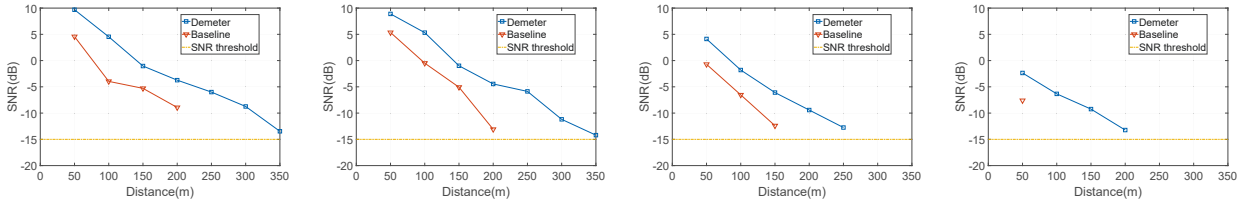

(a) VWC=16% (b) VWC=25% (c) VWC=36% (d) VWC=47%

Figure 16: Impact of moisture to Demeter.

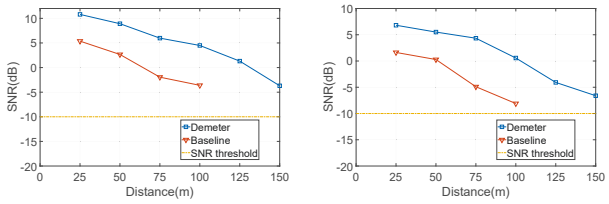

(a) Sandy Loam Soil (b) Clay Soil

Figure 17: Impact of soil type to Demeter.

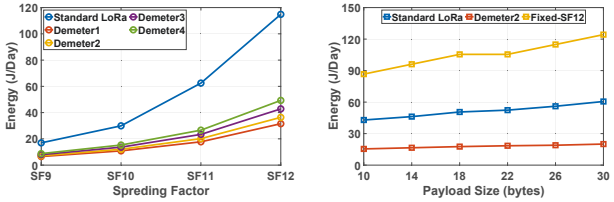

Figure 18: The analysis of energy consumption per day under various settings.

5) Soil Type Experiment Settings: To explore the influence of soil type, we evaluate our system under three agricultural soil types: loam soil, clay soil, and sandy loam soil. The percentages of silt, sand, and clay can categorize soil. Loam has balanced components and good fertility. It holds moisture and nutrients well, drains excess water easily, and allows air to circulate around plant roots, which is ideal for gardening and agriculture. Clay takes the most percentage of clay soil, which has smaller and fewer pore spaces than loam soil, which means that water drains slowly and can cause waterlogging and compaction. Sandy loam soil has more sand compared to loam. It has a coarse texture and a loose structure that allows water and air to flow through easily. In the experiments, the depth is 35 cm and SF is set as 8.

Results: The results for loam soil are shown in Figure 12(b). Figure 17 shows the results for sandy loam and clay soils. Demeter achieves higher SNR in sandy loam of Figure 17(a) than loam with the same horizontal distance while Demeter achieves lower in clay soil of Figure 17(b) than in loam. Baseline signals in sandy loam yield the best performance, while clay soil ones are the worst. The SNR difference between these two types of soil is 3.39 dB. The SNR gain is 6.9 dB, 6.93 dB, and 7.08 dB in loam, sandy loam, and clay soils, respectively. This indicates Demeter can work in multiple types of soils and achieve good communication quality and similar SNR gains.

5.3 Energy Consumption Analysis

Experiment Settings: By leveraging the SNR gain of Demeter, we can increase the data rate with a lower SF to save energy compared to the baseline under the same link budget. Previous experiment results indicate Demeter can achieve at least 5 dB SNR gain, which means we can reduce SF by 2 grades with a lower SNR threshold compared to the standard LoRa [18, 20, 34, 60]. For example, if the standard LoRa has to use SF12, we can use SF10 for packet transmission. Given different link budgets and SF settings, the energy saving for each packet ranges from 0.0569 J to 0.5786 J with 3.3 V voltage.

First, we make a LoRa node sending six packets per hour to evaluate the energy efficiency of Demeter compared to the standard LoRa under different polarization calibration frequencies. Based on the fact that significant fluctuations in SNR occur only 5 times over a 9-day period in Figure 3, we set Θ from 0.5 to 6. Specifically, Demeter 1 triggers the calibration once every two days. Demeter 2, 3, and 4 trigger the calibration 2, 4, and 6 times per day. By default, the payload size is set to 26 bytes. We calculate the energy consumption per day under four different link budgets from SF9 to SF12.

To further verify the performance of various payload lengths, we adopt six payload sizes from 10 bytes to 30 bytes. For each payload size, we calculate the average energy consumption per day of 144 packet transmissions under link budgets from SF9 to SF12 (i.e., 36 packets for each link budget). We compare Demeter 2 with the standard LoRa and Fixed-SF12, which always applies SF12 to transmit packets no matter the current link budget.

Results: In Figure 18(a), Demeter 1–4 outperforms the standard LoRa under different link budgets. For example, compared to the standard LoRa, Demeter 2 reduces energy consumption per day by 68.3% and 57.9% for SF12 and SF9, separately. Moreover, we can see that energy consumption per day increases when calibration trigger frequencies increase. Demeter 1's average energy consumption per day under the four SF settings is 34.1% of the standard LoRa while Demeter 4's increases to 48.5%. Figure 18(b) illustrates the energy consumption under different payload sizes. Demeter 2 reduces energy consumption per day by 82.0% compared to Fixed-SF12 and 63.4% compared to the standard LoRa. For a LoRa node with a 4,400 mAh energy store (i.e., two mid-grade

Alkaline AA batteries), this would extend the system lifetime roughly 5.5×. The results indicate the energy benefits of polarization alignment are far more than the energy cost incurred by alignment calibration in Demeter.

6 RELATED WORK

Cross-soil IoT Systems: Ad-hoc Wireless Underground Sensor Networks (WUSN) [66–68, 77, 90] is well studied for cross-soil IoT. For example, Wang et al. [90] propose a soil measurement system based on WUSN. Dong et al. [17] and Silva et al. [68] present autonomous precision irrigation systems with WUSN. Compared to ad-hoc WUSN, we focus on cross-soil LPWAN, a parallel IoT paradigm. Moreover, some works [10, 36, 97] utilize COTS LoRa and NBIoT to demonstrate the feasibility of cross-soil LPWAN. In comparison, Demeter further enhances the reliability, communication range and depth, and energy efficiency of LoRa cross-soil communication.

In-soil Communication Method: Some works [67, 71, 86, 95] focus on extending the depth a sensor can be buried at with electromagnetic waves [67, 86], magnetic coils [71], and acoustic signals [95]. For example, Sun et al. [71] adopt magnetic induction to reduce signal path loss in soils. The communication system [95] can achieve up to 50 m buried depth with a low-cost acoustic transceiver. Although magnetic and acoustic signals are able to tolerate the signal loss brought by soils, they cannot enable long-range communication over the air, which hampers the farm-scale agricultural data collection needs. In contrast, Demeter is able to achieve much longer cross-soil communication distance for general-purpose agricultural IoT systems.

Polarization-aware Communication for IoT: LLAMA [13] implemented a reconfigurable meta-surface to rotate the polarization of signal between transmitter and receiver. Polartracker [91] and Polarscheduler [35] propose a polarization-aware link model to communicate in polarization-aligned periods. In comparison, Demeter enables adaptive polarization alignment by a customized RF front-end for cross-soil LPWAN with low protocol overhead.

7 DISCUSSION AND FUTURE WORK

VWC range in our field study. Our in-field experiments were conducted just after a wheat harvest. Therefore, no irrigation was applied, leading to lower VWC values than those reported in the growing season [14, 31, 41, 98] in our field study. Although the controlled experiments (e.g., Table 2, Figure 16) demonstrate a consistent performance gain when the VWC increases to 48%, we plan to conduct a large-scale deployment in the next growing season to evaluate Demeter performance in a more realistic VWC.

Hobbyist soil moisture sensor. The soil moisture sensor [47] we used to measure the groundtruth VWC is a hobbyist-level sensor. Although it can correctly report the trend of soil moisture changes, the accuracy of soil moisture measurement is not guaranteed. Since the specific characteristics of the soil greatly influence the accuracy of soil moisture sensors, a more accurate sensor with a soil-specific calibration would be used. In our future work, we will employ a calibratable and accurate professional-level soil moisture sensor for exploring soil-specific polarization calibration.

Adaptive polarization calibration for large-scale deployment One of our future works is to go beyond the physical layer design in this paper to build a reliable and energy-efficient network stack for achieving large-scale deployment. Considering environment and soil diversity in large-scale deployment, different LoRa nodes may need to be calibrated with different schedules. Instead of our periodical polarization calibration, on-demand polarization calibration will play a significant role in large-scale deployment as it allows a LoRa node to calibrate its polarization adaptively. A machine learning based method may be feasible to determine the trigger for a polarization calibration by taking multi-dimensional environmental and soil property changes as inputs. However, it is challenging to balance inference accuracy and computation cost on energy-limited LoRa nodes. Moreover, we will integrate RF front-end circuit design of Demeter to facilitate large-scale deployment and quantify the performance and cost benefits compared to other cross-soil communication solutions.

8 CONCLUSION

In this work, we present Demeter, a novel system that enables reliable cross-soil LPWAN communication. The main contribution of Demeter is a low-cost antenna system that aligns the polarization between LoRa node and gateway antennas and works with COST single RF-chain LPWAN radios. We also develop a low-cost hybrid coupler to encode and change polarization degrees with phase information. Furthermore, we propose a heuristic algorithm to calibrate the polarization alignment automatically. We implement Demeter with customized PCB circuits and COTS devices to evaluate its performance in various soil conditions and scenarios. Demeter can work with various soil types and different environmental conditions. The results show that Demeter can achieve up to 9.94 dB SNR gain outdoors and 11.6 dB indoors, 4× horizontal communication distance, at least 20cm underground depth improvement, and up to 82% energy reduction compared with COTS LoRa node.

ACKNOWLEDGEMENT

We sincerely thank the anonymous reviewers and our shepherd for their valuable feedback. This work was partially supported by NSF Award NeTS-2312674, 2312675, 2312676.

REFERENCES

[1] Nurzaman Ahmed, Debashis De, and Iftekhar Hussain. 2018. Internet of Things (IoT) for smart precision agriculture and farming in rural areas. *IEEE Internet of Things Journal* (2018).

[2] Ian F Akyildiz and Erich P Stuntebeck. 2006. Wireless underground sensor networks: Research challenges. *Ad Hoc Networks* (2006).

[3] LoRa Alliance. [n. d.]. A technical overview of LoRa and LoRaWAN. https://lora-alliance.org/about-lorawan/. Retrieved by Aug 15th, 2023.

[4] Nikolaos G Apergis, Ioannis P Inglesis, Symeon Vasileiadis, and Stelios A Mitilineos. 2019. Development of a small form factor switched-beam antenna for IoT applications at the 868 MHz ISM band. In *Proceedings of APC*.

[5] Srinivasa Balivada, Gregory Grant, Xufeng Zhang, Monisha Ghosh, Supratik Guha, and Roser Matamala. 2022. A wireless underground sensor network field pilot for agriculture and ecology: Soil moisture mapping using signal attenuation. *Sensors* (2022).

[6] Thomas E Berry, Elizabeth Lord, and Cliff Morgan. 2016. Soil polarization data collected for the global undisturbed/disturbed earth (GUIDE) program. In *SPIE Proceedings of Polarization: Measurement, Analysis, and Remote Sensing XII*.

[7] Konstantin Yu Bliokh and Yury P Bliokh. 2006. Conservation of angular momentum, transverse shift, and spin Hall effect in reflection and refraction of an electromagnetic wave packet. *Physical review letters* (2006).

[8] Francois-Marie Breon, Didier Tanre, Pierre Lecomte, and Maurice Herman. 1995. Polarized reflectance of bare soils and vegetation: measurements and models. *IEEE Transactions on Geoscience and Remote Sensing* (1995).

[9] Curtis A Carlson and John L Ingraham. 1983. Comparison of denitrification by Pseudomonas stutzeri, Pseudomonas aeruginosa, and Paracoccus denitrificans. *Applied and Environmental Microbiology* (1983).

[10] German Castellanos, Margot Deruyck, Luc Martens, and Wout Joseph. 2020. System assessment of WUSN using NB-IoT UAV-aided networks in potato crops. *IEEE Access* (2020).

[11] DEQ's Environmental Assistance Center. [n. d.]. Nitrate in Drinking Water. https://www.dhd2.org/wp-content/uploads/2016/12/deq-wd-gws-ciu-nitratebrochure_270430_7.pdf. Retrieved by Aug 14th, 2023.

[12] Nchimunya Chaamwe, Wenyu Liu, and Hongbo Jiang. 2010. Wave propagation communication models for wireless underground sensor networks. In *Proceedings of IEEE ICCT*.

[13] Lili Chen, Wenjun Hu, Kyle Jamieson, Xiaojiang Chen, Dingyi Fang, and Jeremy Gummeson. 2021. Pushing the Physical Limits of IoT Devices with Programmable Metasurfaces. In *Proceedings of USENIX NSDI*.

[14] Sumon Datta, Saleh Taghvaeian, and Jacob Stivers. 2017. *Understanding soil water content and thresholds for irrigation management.* Technical Report. Oklahoma Cooperative Extension Service.

[15] Gabriele Di Renzone, Stefano Parrino, Giacomo Peruzzi, Alessandro Pozzebon, and Duccio Bertoni. 2021. LoRaWAN underground to above-ground data transmission performances for different soil compositions. *IEEE Transactions on Instrumentation and Measurement* (2021).

[16] Doktar. [n. d.]. Filiz: Agricultural Sensor Station. https://www.doktar.com/en/products/agricultural-sensor-station-soil-temperature/. Retrieved by Aug 14th, 2023.

[17] Xin Dong, Mehmet C Vuran, and Suat Irmak. 2013. Autonomous precision agriculture through integration of wireless underground sensor networks with center pivot irrigation systems. *Ad Hoc Networks* (2013).

[18] Adwait Dongare, Revathy Narayanan, Akshay Gadre, Anh Luong, Artur Balanuta, Swarun Kumar, Bob Iannucci, and Anthony Rowe. 2018. Charm: Exploiting Geographical Diversity through Coherent Combining in Low-Power Wide-Area Networks. In *Proceedings of ACM/IEEE IPSN*.

[19] Jialuo Du, Yidong Ren, Mi Zhang, Yunhao Liu, and Zhichao Cao. 2023. NELoRa-Bench: A Benchmark for Neural-enhanced LoRa Demodulation. *arXiv preprint arXiv:2305.01573* (2023).

[20] Jialuo Du, Yidong Ren, Zhui Zhu, Chenning Li, Zhichao Cao, Qiang Ma, and Yunhao Liu. 2023. SRLoRa: Neural-enhanced LoRa Weak Signal Decoding with Multi-gateway Super Resolution. In *Proceedings of ACM MobiHoc*.

[21] Christian Ebi, Fabian Schaltegger, Andreas Rüst, and Frank Blumensaat. 2019. Synchronous LoRa mesh network to monitor processes in underground infrastructure. *IEEE Access* (2019).

[22] EPQ. [n. d.]. Ground Water. https://www.epa.gov/report-environment/ground-water#importance. Retrieved by Aug 15th, 2023.

[23] Rastislav Galuscak-OM6AA and Pavel Hazdra. 2006. Circular polarization and polarization losses.

[24] Robin Gebbers and Viacheslav I Adamchuk. 2010. Precision agriculture and food security. *Science* (2010).

[25] Derek G Groenendyk, Ty PA Ferre, Kelly R Thorp, and Amy K Rice. 2015. Hydrologic-process-based soil texture classifications for improved visualization of landscape function. *PloS one* (2015).

[26] Bernhard Großwindhager, Mustafa S Bakr, Michael Rath, Fabrizio Gentili, Wolfgang Bösch, Klaus Witrisal, Carlo Alberto Boano, and Kay Römer. 2017. Poster: Switchable Directional Antenna System for UWB-based Internet of Things Applications.. In *Proceedings of EWSN*.

[27] Muhammad Abdur Rehman Hashmi and Paul V Brennan. 2023. An Antenna Solution for Glacial Environmental Sensor Networks. *IEEE Access* (2023).

[28] G Hassan, KM Ismail, N Persaud, and RB Reneau Jr. 2004. Dependence of the degree of linear polarization in scattered visible light on soil textural fractions. *Soil science* (2004).

[29] HoBo. [n. d.]. HoBonet Field Monitoring System. https://www.onsetcomp.com/hobonet-field-monitoring-system. Retrieved by Aug 14th, 2023.

[30] Christopher L Holloway, Edward F Kuester, Joshua A Gordon, John O'Hara, Jim Booth, and David R Smith. 2012. An overview of the theory and applications of metasurfaces: The two-dimensional equivalents of metamaterials. *IEEE antennas and propagation magazine* (2012).

[31] Mauro E Holzman, Raul Rivas, and Maria Cintia Piccolo. 2014. Estimating soil moisture and the relationship with crop yield using surface temperature and vegetation index. *International Journal of Applied Earth Observation and Geoinformation* (2014).

[32] Akira Ishimaru. 2017. *Electromagnetic wave propagation, radiation, and scattering: from fundamentals to applications.* John Wiley & Sons.

[33] Nahina Islam, Biplob Ray, and Faezeh Pasandideh. 2020. IoT Based Smart Farming: Are the LPWAN Technologies Suitable for Remote Communication?. In *Proceedings of IEEE SmartIoT*.

[34] Chenning Li, Hanqing Guo, Shuai Tong, Xiao Zeng, Zhichao Cao, Mi Zhang, Qiben Yan, Li Xiao, Jiliang Wang, and Yunhao Liu. 2021. NELoRa: Towards Ultra-low SNR LoRa Communication with Neural-enhanced Demodulation. In *Proceedings of ACM SenSys*.

[35] Ruinan Li, Xiaolong Zheng, Yuting Wang, Liang Liu, and Huadong Ma. 2022. Polarscheduler: Dynamic transmission control for floating lora networks. In *Proceedings of IEEE INFOCOM*.

[36] Kaiqiang Lin and Tong Hao. 2021. Experimental Link Quality Analysis for LoRa-Based Wireless Underground Sensor Networks. *IEEE Internet of Things Journal* (2021).

[37] Marco Mezzavilla, Menglei Zhang, Michele Polese, Russell Ford, Sourjya Dutta, Sundeep Rangan, and Michele Zorzi. 2018. End-to-end simulation of 5G mmWave networks. *IEEE Communications Surveys & Tutorials* (2018).

[38] Thomas A Milligan. 2005. *Modern antenna design*. John Wiley & Sons.
[39] Monnit. [n. d.]. Monnit Agriculture and Livestock Monitoring. https://www.monnit.com/applications/agriculture-livestock-monitoring/. Retrieved by Aug 14th, 2023.
[40] Luca Mottola, Thiemo Voigt, and Gian Pietro Picco. 2013. Electronically-switched directional antennas for wireless sensor networks: A full-stack evaluation. In *Proceedings of IEEE SECON*.
[41] C Nendel, M Berg, K Ch Kersebaum, W Mirschel, X Specka, M Wegehenkel, KO Wenkel, and R Wieland. 2011. The MONICA model: Testing predictability for crop growth, soil moisture and nitrogen dynamics. *Ecological Modelling* (2011).
[42] Mathieu Nicolet, Martin Schnaiter, and Olaf Stetzer. 2012. Circular depolarization ratios of single water droplets and finite ice circular cylinders: a modeling study. *Atmospheric Chemistry and Physics* (2012).
[43] Martin Nilsson. 2009. Directional antennas for wireless sensor networks. In *In Proceedings of Adhoc Workshop*.
[44] Martin Nilsson. 2010. Spida: A direction-finding antenna for wireless sensor networks. In *Proceedings of Springer International Workshop on Real-World Wireless Sensor Networks*.
[45] NSF. [n. d.]. 2022 Signal in the Soils Program Solicitation. https://www.nsf.gov/pubs/2022/nsf22550/nsf22550.htm. Retrieved by Aug 14th, 2023.
[46] Sogo Okamura and Tomohiro Oguchi. 2010. Electromagnetic wave propagation in rain and polarization effects. *Proceedings of the Japan academy, series B* (2010).
[47] PINO-TECH. [n. d.]. SoilWatch 10 – Soil Moisture Sensor. https://pino-tech.eu/soilwatch10/. Retrieved by Aug 15th, 2023.
[48] David M Pozar. 2011. *Microwave engineering*. John wiley & sons.
[49] pSemi. [n. d.]. pe44820. https://www.psemi.com/products/rf-phase-amplitude-control/phase-shifters/pe44820. Retrieved by Aug 15th, 2023.
[50] Nicolas Quintana-Ashwell, Drew Gholson, Gurpreet Kaur, Gurbir Singh, Joseph Massey, L Jason Krutz, Christopher G Henry, Trey Cooke III, Michele Reba, and Martin A Locke. 2022. Irrigation Water Management Tools and Alternative Irrigation Sources Trends and Perceptions by Farmers from the Delta Regions of the Lower Mississippi River Basin in South Central USA. *Agronomy* (2022).
[51] Yidong Ren, Li Liu, Chenning Li, Zhichao Cao, and Shigang Chen. 2022. Is LoRaWAN Really Wide? Fine-grained LoRa Link-level Measurement in An Urban Environment. In *Proceedings of IEEE ICNP*.
[52] ABI Research. [n. d.]. NB-IoT and LTE-M Issues to Boost LoRa and Sigfox Near and Long-term Lead in LPWA Network Connections. https://tinyurl.com/2026-cellular-iot. Retrieved by Aug 15th, 2023.
[53] Ettus Research. [n. d.]. SBX 400-4400 datasheet. https://www.ettus.com/all-products/sbx/. Retrieved by Aug 15th, 2023.
[54] Ettus Research. [n. d.]. USRP N210 datasheet. https://www.ettus.com/all-products/un210-kit/. Retrieved by Aug 15th, 2023.
[55] Abdul Salam and Usman Raza. 2020. *Signals in the Soil*. Springer.
[56] Abhijit Sarkar. 1981. Change of Polarization of Electromagnetic Waves on Reflection From Planar Interfaces. *IETE Journal of Research* (1981).
[57] Javier Schandy, Simon Olofsson, Nicolas Gammarano, Leonardo Steinfeld, and Thiemo Voigt. 2021. Improving sensor network performance with directional antennas: A cross-layer optimization. *ACM Transactions on Sensor Networks* (2021).
[58] Semtech. [n. d.]. LoRa and LoRaWAN. https://lora-developers.semtech.com/documentation/tech-papers-and-guides/lora-and-lorawan/. Retrieved by Aug 15th, 2023.
[59] Semtech. [n. d.]. Semtech. https://www.semtech.com/. Retrieved by Aug 15th, 2023.
[60] Semtech. [n. d.]. SX1276 datasheet. https://www.semtech.com/products/wireless-rf/lora-connect/sx1276. Retrieved by Aug 15th, 2023.
[61] Semtech. [n. d.]. SX1302. https://www.semtech.com/products/wireless-rf/lora-core/sx1302. Retrieved by Aug 15th, 2023.
[62] Semtech. [n. d.]. sx1302cfd915gw1h. https://www.semtech.com/products/wireless-rf/lora-core/sx1302cfd915gw1h. Retrieved by Aug 15th, 2023.
[63] Semtech. [n. d.]. SX1303. https://www.semtech.com/products/wireless-rf/lora-core/sx1303. Retrieved by Aug 15th, 2023.
[64] Joseph A Shaw. 1999. Degree of linear polarization in spectral radiances from water-viewing infrared radiometers. *Applied optics* (1999).
[65] Ching-Ian Shie, Jui-Ching Cheng, Sheng-Chun Chou, and Yi-Chyun Chiang. 2009. Transdirectional Coupled-Line Couplers Implemented by Periodical Shunt Capacitors. *IEEE Transactions on Microwave Theory and Techniques* (2009).
[66] Agnelo R Silva and Mehmet C Vuran. 2009. Empirical evaluation of wireless underground-to-underground communication in wireless underground sensor networks. In *Proceedings of DCOSS*.
[67] Agnelo R Silva and Mehmet Can Vuran. 2010. Communication with aboveground devices in wireless underground sensor networks: An empirical study. In *Proceedings of IEEE ICC*.
[68] Agnelo R Silva and Mehmet C Vuran. 2010. CPS^2: integration of center pivot systems with wireless underground sensor networks for autonomous precision agriculture. In *Proceedings of ACM/IEEE ICCPS*.
[69] Julius Adams Stratton. 2007. *Electromagnetic theory*. Vol. 33. John Wiley & Sons.
[70] Zhi Sun and Ian F Akyildiz. 2010. Connectivity in wireless underground sensor networks. In *Proceedings of IEEE SECON*.
[71] Zhi Sun and Ian F Akyildiz. 2010. Magnetic induction communications for wireless underground sensor networks. *IEEE transactions on antennas and propagation* (2010).
[72] Tomonori Tanikawa, Kazuhiko Masuda, Hiroshi Ishimoto, Teruo Aoki, Masahiro Hori, Masashi Niwano, Akihiro Hachikubo, Sumito Matoba, Konosuke Sugiura, Takenobu Toyota, et al. 2021. Spectral degree of linear polarization and neutral points of polarization in snow and ice surfaces. *Journal of Quantitative Spectroscopy and Radiative Transfer* (2021).
[73] Giovani Tarter, Luca Mottola, and Gian Pietro Picco. 2016. Directional antennas for convergecast in wireless sensor networks: Are they a good idea?. In *Proceedings of IEEE MASS*.
[74] VV Temnov, K Sokolowski-Tinten, P Zhou, A El-Khamhawy, and D Von Der Linde. 2006. Multiphoton ionization in dielectrics: comparison of circular and linear polarization. *Physical review letters* (2006).
[75] Bee Yen Toh, Robert Cahill, and Vincent F Fusco. 2003. Understanding and measuring circular polarization. *IEEE Transactions on Education* (2003).
[76] Shuai Tong, Jiliang Wang, Jing Yang, Yunhao Liu, and Jun Zhang. 2023. Citywide LoRa Network Deployment and Operation: Measurements, Analysis, and Implications. In *Proceedings of ACM SenSys*.
[77] John Tooker, Xin Dong, Mehmet C Vuran, and Suat Irmak. 2012. Connecting soil to the cloud: A wireless underground sensor network testbed. In *Proceedings of IEEE SECON*.
[78] USDA. Retrieved by Dec 27th 2023. Soil Texture Calculator.
[79] USDA. Retrieved by Dec 27th 2023. Web Soil Survey.
[80] USEPA. [n. d.]. Estimated Nitrate Concentrations in Groundwater Used for Drinking. https://www.epa.gov/nutrient-policy-data/estimated-nitrate-concentrations-groundwater-used-drinking. Retrieved by Aug 15th, 2023.
[81] USEPA. [n. d.]. Overview of Greenhouse Gases. https://www.epa.gov/ghgemissions/overview-greenhouse-gases. Retrieved by Aug 15th, 2023.

[82] JD Van der Laan, DA Scrymgeour, SA Kemme, and EL Dereniak. 2015. Detection range enhancement using circularly polarized light in scattering environments for infrared wavelengths. *Applied optics* (2015).

[83] John D van der Laan, Jeremy Benjamin Wright, Shanalyn A Kemme, and David A Scrymgeour. 2018. Superior signal persistence of circularly polarized light in polydisperse, real-world fog environments. *Applied Optics* (2018).

[84] John D van der Laan, Jeremy B Wright, David A Scrymgeour, Shanalyn A Kemme, and Eustace L Dereniak. 2015. Evolution of circular and linear polarization in scattering environments. *Optics Express* (2015).

[85] Deepak Vasisht, Zerina Kapetanovic, Jongho Won, Xinxin Jin, Ranveer Chandra, Sudipta Sinha, Ashish Kapoor, Madhusudhan Sudarshan, and Sean Stratman. 2017. FarmBeats: An IoT Platform for Data-Driven Agriculture. In *Proceedings of USENIX NSDI*.

[86] Jose Vasquez, Victor Rodriguez, and David Reagor. 2004. Underground wireless communications using high-temperature superconducting receivers. *IEEE Transactions on Applied Superconductivity* (2004).

[87] Mehmet C Vuran and Ian F Akyildiz. 2010. Channel model and analysis for wireless underground sensor networks in soil medium. *Physical communication* (2010).

[88] M Can Vuran and Agnelo R Silva. 2009. Communication through soil in wireless underground sensor networks–theory and practice. *Sensor networks: Where theory meets practice* (2009).

[89] Xue-fen Wan, Yi Yang, Jian Cui, and Muhammad Sohail Sardar. 2017. Lora propagation testing in soil for wireless underground sensor networks. In *Proceedings of IEEE APCAP*.

[90] Qiang Wang, Andreas Terzis, and Alex Szalay. 2010. A novel soil measuring wireless sensor network. In *Proceedings of IEEE I2MTC*.

[91] Yuting Wang, Xiaolong Zheng, Liang Liu, and Huadong Ma. 2021. PolarTracker: Attitude-aware Channel Access for Floating Low Power Wide Area Networks. In *Proceedings of IEEE INFOCOM*.

[92] WAVEFORM. [n. d.]. 2x2 Cross-Polarized 600-2700 MHz Outdoor Antenna. https://www.waveform.com/products/2x2-mimo-outdoor-panel-antenna. Retrieved by Aug 15th, 2023.

[93] XRDS-RF. [n. d.]. 3dB XRDS-RF 698-2700MHz passive splitter. https://www.amazon.com/Wide-Band-Splitter-3dB-Type-Female-50-XRDS-RF/dp/B07V6YH8BV. Retrieved by Aug 15th, 2023.

[94] Kang Yang, Yuning Chen, Xuanren Chen, and Wan Du. 2023. Link Quality Modeling for LoRa Networks in Orchards. In *Proceedings of IEEE/ACM IPSN*.

[95] Sijung Yang, Omar Baltaji, Andrew C Singer, and Youssef MA Hashash. 2019. Development of an underground through-soil wireless acoustic communication system. *IEEE Wireless Communications* (2019).

[96] Yanbo Zhang, Weiping Sun, Yidong Ren, Sung-ju Lee, and Mo Li. 2022. Channel Adapted Antenna Augmentation for Improved Wi-Fi Throughput. *IEEE Transactions on Mobile Computing* (2022).

[97] Baofeng Zhou, Venkat Sai Suman Lamba Karanam, and Mehmet C. Vuran. 2021. Impacts of Soil and Antenna Characteristics on LoRa in Internet of Underground Things. In *Proceedings of IEEE GLOBECOM*.

[98] Qing Zhu and Henry Lin. 2011. Influences of soil, terrain, and crop growth on soil moisture variation from transect to farm scales. *Geoderma* (2011).